JOURNAL OF SPACECRAFT AND ROCKETS
Vol. 35, No. 5, September–October 1998

Minimum Heating Entry Trajectories for Reusable Launch Vehicles

Robert Windhorst* and Mark Ardema†
Santa Clara University, Santa Clara, California 95053
and
Jeffrey Bowles‡
NASA Ames Research Center, Moffett Field, California 94035

A finite control volume heat transfer analysis is coupled to a flight-path optimization and integration algorithm for the purpose of calculating conductive heat rates and transient temperature effects within the thermal protection system of a reusable launch vehicle. Results are obtained for three different thermal protection system concepts: tile, blanket, and metallic. The optimization algorithm is based on the energy state approximation and is used to generate optimal entry trajectories minimizing the following three criteria: 1) the thermal energy absorbed at the vehicle surface, 2) the heat load applied to the vehicle, and 3) the thermal energy absorbed by the internal structure. Results indicate that all three trajectories produce comparable peak internal structure temperatures for a given thermal protection system, with the trajectory minimizing the heat load applied to the vehicle producing the lowest peak temperature. However, if the maximum stagnation temperature constraint at the nose of the vehicle is increased from 3000 to 4000°F, the trajectory minimizing the thermal energy absorbed by the internal structure becomes superior. Further, the trajectory with the 4000°F limit gives a peak internal structure temperature 25°F less than the one with the 3000°F limit.

Nomenclature

c = specific heat, btu/(lb · R)
D = drag, lb
dt = time step required by vehicle to travel between energy levels, s
E = specific energy, ft
g_s = gravitational acceleration at the Earth's surface, ft/s^2
h = altitude, ft
k = thermal conductivity, btu/(h · ft · R)
L = total thickness of thermal protection system (TPS)
P = specific excess power, ft/s
P_{surf} = pressure at vehicle surface, lb/ft^2
Q_{abs} = thermal energy conducted per square foot, btu/ft^2
$\dot{Q}_{abs}$ = conductive heat rate per square foot, btu/(h · ft^2)
Q_{conv} = thermal energy convected per square foot, btu/ft^2
$\dot{Q}_{conv}$ = convective heat rate per square foot, btu/(h · ft^2)
Q_{rad} = thermal energy radiated per square foot, btu/ft^2
$\dot{Q}_{rad}$ = radiative heat rate per square foot, btu/(h · ft^2)
q = dynamic pressure, lb/ft^2
R = radius of the Earth, ft
T = thrust, lb
T_i = temperature of TPS node i, °F
T_{surf} = estimated temperature at vehicle surface, °F
t = flight time, min
v = speed, ft/s
x = TPS depth measured from surface, in.
ε = emissivity
ρ = density, lb/ft^3
σ = Stefan–Boltzmann constant, btu/(h · ft^2 · R^4)
Φ = integrated optimization function
$\dot{\Phi}$ = optimization function

Received Oct. 24, 1997; revision received April 20, 1998; accepted for publication May 8, 1998.

*Research Assistant, Department of Mechanical Engineering. Student Member AIAA.
†Professor and Chairman, Department of Mechanical Engineering. Associate Fellow AIAA.
‡Aerospace Engineer, Systems Analysis Branch. Member AIAA.

Introduction

CURRENT research and development of advanced reusable launch vehicles (RLVs) focus on reducing the cost of access to space and the turnaround time between missions. The RLV program proposes to reduce operating cost and turnaround in part by redesigning the vehicle thermal protection system (TPS) for lighter weight, reusability, and increased durability relative to the Space Shuttle. There are two key interrelated aspects of launch vehicle TPS design: optimizing the vehicle re-entry trajectory for minimum internal structure temperatures for a given TPS and evaluating advanced, lightweight, reusable TPS materials. Although this report concentrates on the trajectory optimization problem, results are given for three different TPS concepts: tile, blanket, and metallic. The tile and blanket TPS concepts are similar to what is currently used on the Space Shuttle. The underside of the Shuttle uses a tile TPS, and the top side uses a blanket TPS. The metallic TPS, however, represents a new concept designed for the goals just mentioned: lighter weight, reusability, and increased durability.

As an RLV descends into the atmosphere from orbit, it undergoes extreme convective heat rates $\dot{Q}_{conv}$ due to its high kinetic energy. The magnitude and duration of $\dot{Q}_{conv}$ determine the thickness of the TPS required to prevent the temperature of the vehicle's internal structure from exceeding its limit. In Ref. 1 this problem is approached by using the energy state trajectory approximation[2–5] to minimize the required thickness of the TPS by minimizing the integrated convective heat rate Q_{conv}, also called heat load, applied to the vehicle.

Sachs and Dinkelmann[6] minimize fuel consumption of a hypersonic vehicle subject to a thermal energy absorption constraint. The vehicle is an air-breathing first stage of a two-stage launch system. Because the maximum speed is Mach 6, the kinetic energies and $\dot{Q}_{conv}$ of this vehicle are much lower than those for the entry of a single-stage vehicle. The constraint on the thermal energy absorbed by the vehicle used in Ref. 6 is

$$\int_0^{t_f} \dot{Q}_{abs}\, dt \le Q_{limit}$$

where $\dot{Q}_{abs}$ is the conductive heat rate of the innermost layer of the insulation and is determined by a finite difference heat transfer code much like the one used in the present paper. Because the integral is evaluated at the end of the mission, Sachs and Dinkelmann must

solve a two-point-boundary-value trajectory optimization problem. They found that thermal energy absorbed could be greatly reduced with only a small penalty in fuel consumption.

The approach used in this paper avoids the complexity of the two-point-boundary-value problem (2PBVP) by using the energy state approximation (ESA) technique.[2–5] By the ESA technique, optimal trajectories minimizing a variety of different functions can be generated with a single integration of the equations of motion over the vehicle flight path. Furthermore, ESA techniques could be used to develop an onboard algorithm that uses position feedback to generate optimal trajectories in real time.[5] This paper presents results of optimal trajectories minimizing 1) the thermal energy absorbed Q_{abs} by the RLV at its surface, 2) the heat load Q_{conv} applied to the vehicle (as is done in Ref. 1), and 3) the thermal energy absorbed by the RLV internal structure and compares them to results obtained by minimizing the vehicle descent time and surface temperatures. The goal is to determine which trajectory minimizes the peak internal structure temperature of the RLV for a given thermal protection system. Note that items 1 and 3 are not the same. Not all of the thermal energy absorbed at the RLV surface reaches the internal structure; part of this energy is stored in the capacitance of the thermal protection layer between the surface and internal structure. This stored thermal energy may be further conducted into the internal structure or may be conducted back to the surface, where it radiates off of the RLV. Also discussed are the assumed vehicle constraints on the flight trajectory, the method of generating approximate optimal trajectories, and the equations for calculating temperatures and conductive heat rates $\dot{Q}_{abs}$.

Methods

Vehicle Synthesis Code

The NASA Ames Research Center Hypersonic Aircraft Vehicle Optimization Code (HAVOC) generated all of the optimal trajectories presented in this paper. HAVOC aides RLV design by synthesizing key vehicle elements such as geometry, aerodynamics, dynamics, propulsion, and structures into a single code. The integration of all of these elements into a single code creates a versatile platform ideal for studying RLV optimal trajectories. Furthermore, the code contains built-in subroutines that use ESA techniques to generate near-optimal trajectories minimizing time, fuel, Q_{conv}, Q_{abs}, or a weighted combination of these.[1] Although the optimal paths are determined from ESA methods, the trajectory integration in HAVOC uses a point mass model assuming a spherical rotating Earth with no winds and a flight-path angle rate of zero. The equations of motion are listed as Eq. (1) in Ref. 1.

Constraints

There are seven vehicle constraints imposed on the flight trajectories. Each constraint, along with its upper and/or lower limit, is listed in Table 1. The first constraint is imposed on the dynamic pressure q of the vehicle. Three temperature constraints are imposed at three different locations on the vehicle body. The stagnation temperature constraint at the vehicle nose is TSTAGN. Temperature lower surface (TLS) is the temperature constraint of a point located along the windward surface, centerline, and one-third of the vehicle length from the nose; and temperature upper surface (TUS) is the temperature constraint of a point located along the leeward surface, centerline, and one-third of the vehicle length from the nose. The load factor (SLDFAC) constraint limits the acceleration of the vehicle in the direction normal to the velocity vector. The constraint on the vehicle's angle of attack is AN, and the constraint on the vehicle's flight path angle is FA.

Table 1 Vehicle constraints imposed on flight trajectory

Constraint	Flight parameter constrained	TPS type	Lower limit	Upper limit
q	Dynamic pressure, lb/ft^2	All	20	900
TSTAGN	Stagnation temperature at vehicle nose cap, °F	Carbon carbon	——	3000
TLS	Temperature of lower vehicle surface, °F	Tile	——	2400
		Blanket	——	2000
		Metallic	——	1800
TUS	Temperature of upper vehicle surface, °F	All	——	1200
SLDFAC	Load factor	All	0	2
AN	Vehicle angle of attack, deg	All	−60	+60
FA	Vehicle flight path angle, deg	All	−45	+45

Energy State Approximation

The ESA assumes that the mechanical energy per unit weight of the vehicle

$$E = [hR/(R+h)] + (1/2g_s)v^2$$

is on a slower timescale than the altitude, velocity, and temperature state variables. Thus the other state variable rates may be neglected as compared with a new state variable rate formed by taking the derivative of E with respect to time:

$$P = \frac{\mathrm{d}E}{\mathrm{d}t} = v\frac{(T-D)}{mg_s} \tag{1}$$

The goal of the optimization is to find a trajectory minimizing a specified cost functional

$$\Phi = \int \dot{\Phi}\,\mathrm{d}t \tag{2}$$

Generally, finding such a trajectory requires use of the maximum principle resulting in a 2PBVP. Use of the ESA, however, reduces the problem to one of minimizing a function. Now that there is a single state equation, Eq. (1) may be solved for dt and substituted into Eq. (2):

$$\Phi = \int \dot{\Phi}\frac{\mathrm{d}E}{P} \tag{3}$$

Thus $\dot{\Phi}/P$ is to be minimized at every value of E along the trajectory. We note also that E is preferable to t as an integration variable because its total change is the same for every trajectory.

Temperature Estimation

A surface energy balance calculation, equating the convective heat rate with the radiative heat rate at the surface of the RLV, produces an estimate of the surface temperature T_{surf} as a function of $\dot{Q}_{conv}$. The RLV is divided into multiple surface panels, and engineering approximations are used to construct, for each surface panel, $\dot{Q}_{conv}$ as a function of angle of attack, altitude, and Mach number. The equation for T_{surf} of a given surface panel is derived from the following:

$$\dot{Q}_{conv} = \dot{Q}_{rad} \tag{4}$$

$$\dot{Q}_{conv} = \varepsilon\sigma\left(T_{surf}^4 - T_{amb}^4\right) \tag{5}$$

Solving for T_{surf},

$$T_{surf} = \left(\frac{\dot{Q}_{conv}}{\varepsilon\sigma} + T_{amb}^4\right)^{\frac{1}{4}} \tag{6}$$

In this case T_{surf} is much greater than T_{amb}, and so T_{amb} may be neglected, and T_{surf} becomes a function of $\dot{Q}_{conv}$ only. Equation (6) provides a quick and convenient method of calculating T_{surf} that has been used in past studies of RLV entry heating. Specifically, this approximation for T_{surf} is used in Ref. 1 and does have a drawback. The absence of conduction terms in the surface energy balance equation slightly inflates T_{surf} and, more importantly, does not predict the conductive heat rates $\dot{Q}_{abs}$ and transient temperature effects within the TPS system. As we shall see later, the peak internal structure temperature depends primarily on the latter two.

Heat Transfer Analysis

Calculation of $\dot{Q}_{abs}$ and transient temperature effects within the TPS requires knowledge of surface panel pressure, past TPS temperatures, and a time step in addition to $\dot{Q}_{conv}$. Thermal energy absorbed at the surface is calculated by integrating $\dot{Q}_{abs}$ at the surface, and thermal energy absorbed by the internal structure is calculated by integrating $\dot{Q}_{abs}$ at the beginning of the internal structure. All heat transfer analysis is performed for a single surface panel on the vehicle. For this study, the panel is located at the same place as the TLS temperature constraint, along the windward surface, centerline, and one-third of the vehicle length from the nose.

We solve the one-dimensional heat equation

$$\rho c\frac{\partial T}{\partial t} - \frac{\partial}{\partial x}\left(k\frac{\partial T}{\partial x}\right) = 0 \tag{7}$$

where

$$T = f(x,t), \qquad 0 \le x \le L \tag{8}$$

$$c = f(T), \qquad 0 \le t < \infty \tag{9}$$

$$k = f(T, P_{surf}) \tag{10}$$

Equation (7) is a partial differential equation with, in this case, the initial condition

$$T(x,0) = 70^{\circ}\text{F} \tag{11}$$

and boundary conditions, at $x = 0$,

$$-k\frac{\partial T}{\partial x} = \dot{Q}_{conv} - \varepsilon\sigma\left(T^4 - T_{amb}^4\right) \tag{12}$$

and at $x = L$,

$$-k\frac{\partial T}{\partial x} = 0 \tag{13}$$

The 70°F initial temperature arises from what is currently done with the Space Shuttle. Just before the Shuttle leaves orbit to make its descent, it performs a series of 360-deg rolls in the sun. These rolls are intended to create an even temperature distribution around the shuttle TPS of approximately 70°F. The TPS surface boundary condition at $x = 0$ imposes the law of conservation of energy, forcing the sum of $\dot{Q}_{conv}$, $\dot{Q}_{rad}$, and $\dot{Q}_{abs}$ at the surface to zero. The tank TPS boundary condition at $x = L$ is adiabatic. The adiabatic boundary condition arises from the assumption of a dry tank wall. This assumption is justified by the fact that the vehicle has used up all of its fuel during ascent. Because the fuel tank is empty, any thermal energy reaching the tank has nowhere to go and therefore can only be used in heating the tank structure.

Numerical techniques are used to generate solutions to Eq. (7). A one-dimensional section of the TPS is divided into n number of nodes. Figure 1 illustrates a general nodal breakdown of a TPS section and the five different types of nodes: inner layer nodes, TPS surface boundary nodes, TPS tank boundary nodes, layer boundary nodes, and layer boundary nodes with an air or vacuum gap. Table 2 lists for each TPS the number of layers, layer thickness, layer material, layer weight, and number of inner layer nodes in each layer. The internal structure layer is listed for each TPS in Table 2 as the aluminum layer. All other layers make up the thermal protection between the RLV surface and internal structure. Equation (7) is discretized using the control volume formulation, resulting in a set of n equations, one for each node, and n unknowns, the temperature of each node.[7]

The discretized equation for each type of node is as follows:

1) Inner layer node

$$(k_e/\Delta x)(T_{i+1} - T_i) - (k_e/\Delta x)(T_i - T_{i-1}) = (\rho c/\Delta t)(T_i - T_{i,past}) \tag{14}$$

2) TPS surface boundary node at $x = 0$

$$-(k_e/\Delta x)(T_2 - T_1) = \dot{Q}_{conv} - \varepsilon\sigma\left(T_1^4 - T_{amb}^4\right) \tag{15}$$

Table 2 TPS material and nodal breakdown

TPS	Layer	Material	No. of nodes	Depth, in.	Weight, lb/ft^2
Tile	1	TUFI (toughened unipiece insulation)	5	0.1	0.5
	2	AETB12 (alumina-enhanced thermal barrier)	5	2.0	2.008
	3	RTV-560 (glue)	1	0.012	0.088
	4	Aluminum	1	0.08	1.167
Total			12	2.192	3.763
Blanket	1	TABI (tailorable advanced blanket insulation)	5	2.0	1.550
	2	RTV-560 (glue)	1	0.012	0.088
	3	Aluminum	1	0.08	1.167
Total			7	2.092	2.805
Metallic	1	Inconel 617 honeycomb sandwich	5	0.29	0.628
	2	Q-fiber felt	5	3.5	1.020
	3	Titanium honeycomb sandwich	1	0.18	0.363
	4	Air (gap)	1	0.5	——
	5	Aluminum	1	0.08	1.167
Total			13	4.55	3.178

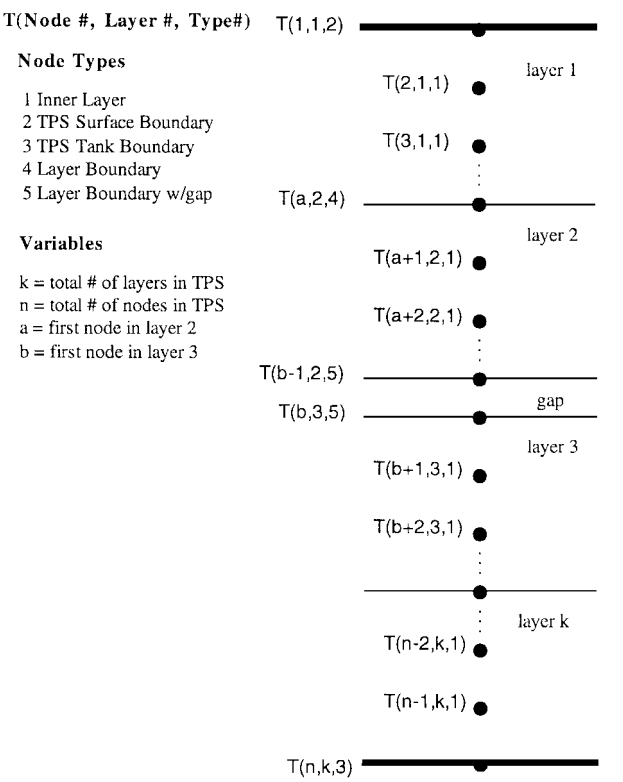

Fig. 1 TPS nodal breakdown.

3) TPS tank boundary node at $x = L$

$$T_n - T_{n-1} = 0 \tag{16}$$

4) Layer boundary node

$$(k_e/\Delta x)(T_{i+1} - T_i) - (k_e/\Delta x)(T_i - T_{i-1}) = 0 \tag{17}$$

5) Layer boundary node with a gap

Equation for gap upper surface node T_i:

$$-(k_e/\Delta x)(T_i - T_{i-1}) = \varepsilon_e\sigma\left(T_i^4 - T_{i+1}^4\right) + h_\infty(T_i - T_{i+1}) \tag{18}$$

Equation for gap lower surface node T_{i+1}:

$$-(k_e/\Delta x)(T_{i+2} - T_{i+1}) = \varepsilon_e\sigma\left(T_i^4 - T_{i+1}^4\right) + h_\infty(T_i - T_{i+1}) \tag{19}$$

where k_e is the interface conductivity.[7] These equations are linearized, grouped into a matrix, and solved for the nodal temperatures.

Once the nodal temperatures are known, $\dot{Q}_{abs}$ may be calculated by Eq. (20). Equation (21) calculates $\dot{Q}_{abs}$ at the vehicle surface, whereas Eq. (22) calculates $\dot{Q}_{abs}$ at the vehicle structure. The subscript m in Eq. (22) denotes the layer boundary node between the aluminum internal structure layer and the layer just before it:

$$\dot{Q}_{abs} = -k\frac{\partial T}{\partial x} \tag{20}$$

$$\dot{Q}_{abs,surf} = -(k/\Delta x)(T_2 - T_1) \tag{21}$$

$$\dot{Q}_{abs,tank} = -(k/\Delta x)(T_{m+1} - T_m) \tag{22}$$

Results

All of the results given in this paper are for a single-stage-to-orbit (SSTO) RLV configuration. Figure 2 illustrates the SSTO RLV configuration and points out the locations of the three temperature constraints imposed on the vehicle.

Minimum Time and Temperature Trajectories

Before considering minimum heating trajectories, minimum time and minimum estimated lower surface temperature trajectories were computed. These are of interest because, loosely speaking, minimum heating trajectories are a weighted sum of time and temperature trajectories. The optimization criteria for these two cases are as follows:

Minimum time

$$\text{minimize} \int \mathrm{d}t$$

Minimum temperature

$$\text{minimize } T_{surf}$$

As expected, the minimum time ESA trajectory (with no banking) follows the highest possible dynamic pressure q path, being limited by maximum stagnation temperature at Mach numbers higher than 15 and by maximum dynamic pressure below that (Fig. 3 and Table 3). Table 3 shows that the descent time for this trajectory was 26 min, the heat load was 5704 Btu/ft^2, and the maximum internal structure temperatures ranged from 267 to 337°F for the three TPS concepts. Reference 1 shows that the descent time can be substantially reduced by bank angle chattering.

The minimum estimated lower surface temperature results are also shown in Fig. 3 and Table 3. The surface temperature is estimated at a point one-third back from the nose on the windward side of the vehicle. This trajectory follows the minimum dynamic pressure constraint, has a descent time of 40 min, produces a heat load of 3708 Btu/ft^2, and gives a range of 271–355°F for the peak internal structure temperature. In Ref. 1 contours of surface temperature for an RLV are plotted in the flight envelope. It was found, generally speaking, that there are regions of relatively low temperature near both the low and high q boundaries with higher values at intermediate values of q. The temperatures in the low q region, however, are lower than those in the high q region, which agrees with our results. This pattern of minimum time and temperature trajectories means that minimum heating trajectories will be on or near either the low q or high q boundaries.

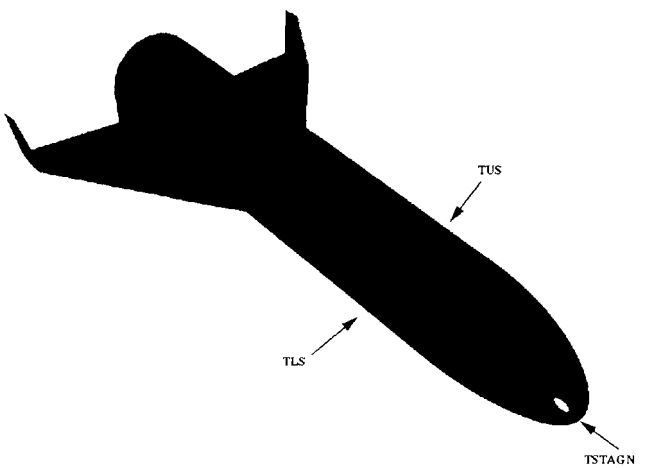

Fig. 2 SSTO RLV configuration.

Table 3 Temperature and time results of optimal trajectories

Case	Descent time, min	Trajectory type	Heat load, Btu/ft^2	Peak structure temperature, °F		
				Tile	Blanket	Metallic
Min. time	26	High q	5704	267	287	337
Min. temp.	40	Low q	3708	272	271	355
1	42	Low q	4135	271	267	353
2	33	Low q	3706	255	253	329
3	26	High q	5871	267	287	337
3*	16	High q	4896	230	——	——

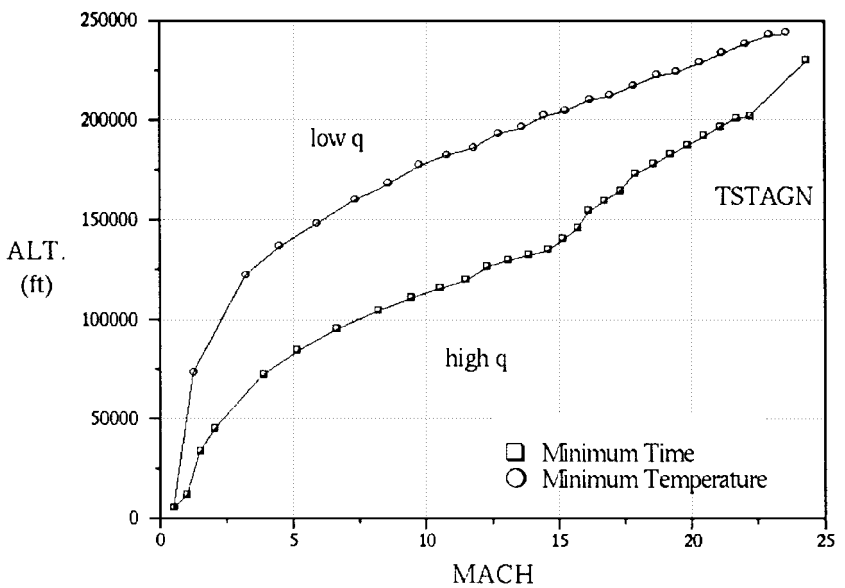

Fig. 3 Entry trajectory profiles for minimum time and minimum temperature.

Minimum Heating Trajectories

The main purpose of the TPS is to limit the interior structure temperature to some maximum acceptable value. Because the peak temperature is not known until the end of the trajectory (indeed, the peak internal structure temperature typically occurs after the vehicle has landed), the coupled problem of sizing the insulation and determining the optimal trajectory is by nature an iterative one. It is the goal of this paper to formulate and evaluate ESA criteria that give noniterative approximations to the trajectory optimization part of this problem.

Three optimization criteria will be investigated in the following sections: case 1—minimize $\int \dot{Q}_{abs}\, dt$ at the surface of the TPS, Eq. (21); case 2—minimize $\int T_{surf}^4\, dt$, Eq. (5); and case 3—minimize $\int \dot{Q}_{abs}\, dt$ at the internal structure, Eq. (22). The integral in case 2 was the criterion used in Ref. 1 and is directly proportional to Q_{conv}. Case 3 was the criterion used in Ref. 6.

Figure 4 shows the trajectories in the flight envelope for the three cases, and Figs. 5 and 6 show their time and estimated surface temperature histories, respectively. Note that Figs. 5 and 6 are plotted using specific energy as the independent variable and illustrate that the total change in specific energy of each case is the same, whereas the change in flight time is not. According to Fig. 4, two of the trajectories, cases 1 and 2, are of the low q type and the other, case 3, is of the high q type. Figures 5 and 6 show that, relative to the high q type, the low q trajectories have long descent times and low surface temperature. They also have high angle of attack and low drag. Table 3 shows, however, that all three cases give peak internal structure temperatures that are very similar, with case 2 giving the best (lowest) value. Also shown in Fig. 4 for reference is the Space Shuttle trajectory[8]; it is seen that this is of the low q type.

The time histories of the convective heat rates are shown in Fig. 7. Figure 7 again illustrates the different natures of the high q and low q trajectories. Notice that the magnitude of $\dot{Q}_{conv}$ for the high q trajectory is much greater and lasts for a shorter time period relative to the magnitude of $\dot{Q}_{conv}$ for the low q trajectories. Table 3 lists the heat load Q_{conv} for each case studied. The heat loads are calculated by taking the area under the curves in Fig. 7. In general, the low q trajectories have lower heat loads, with case 2 having the lowest heat load of 3706 Btu/ft^2. Furthermore, the heat loads do not correspond well with the minimum peak internal structure temperatures; that is, cases with high heat loads do not always have high peak structure temperatures and vice versa.

Figures 8–10 show the time histories of the thermal energy absorbed at the vehicle surface for the three cases and the three TPSs.

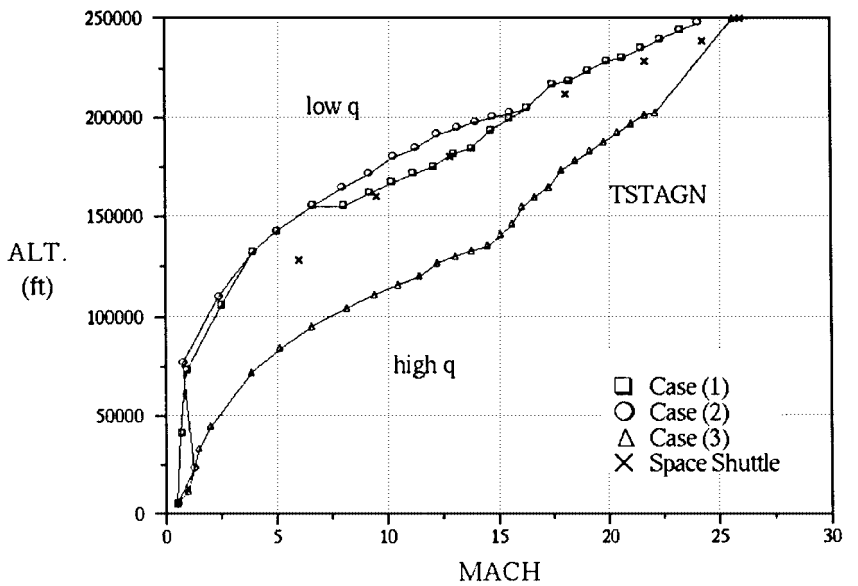

Fig. 4 Entry trajectory profiles for minimum heating.

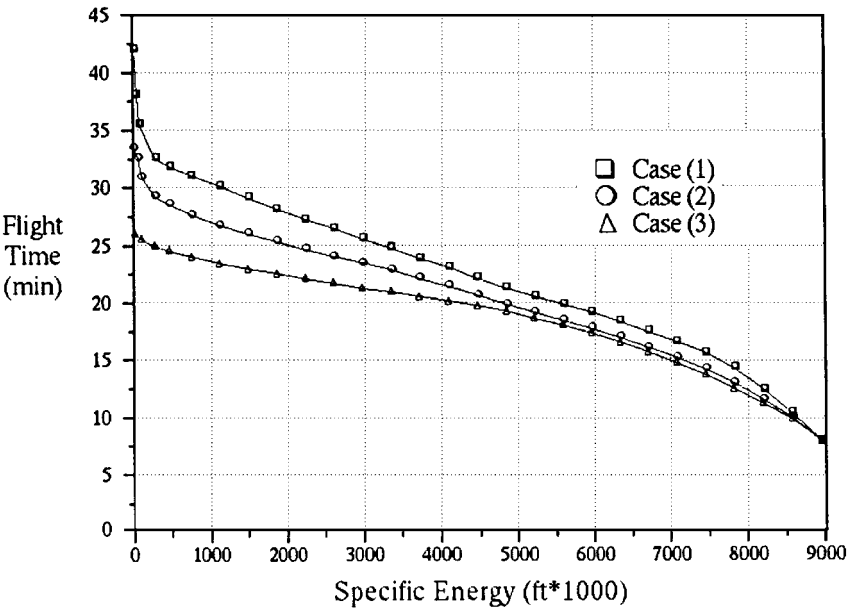

Fig. 5 Flight time vs specific energy.

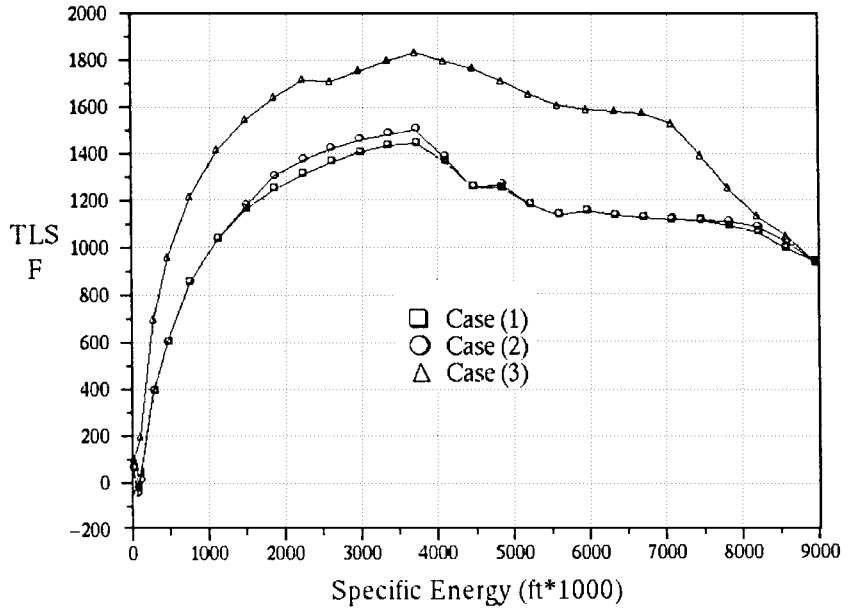

Fig. 6 Estimated surface temperature vs specific energy.

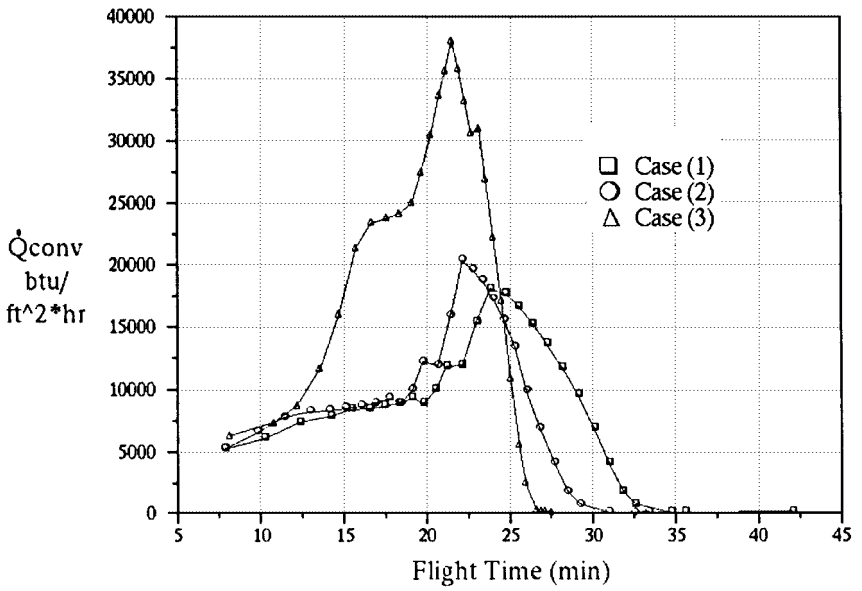

Fig. 7 Convective heat rate vs flight time.

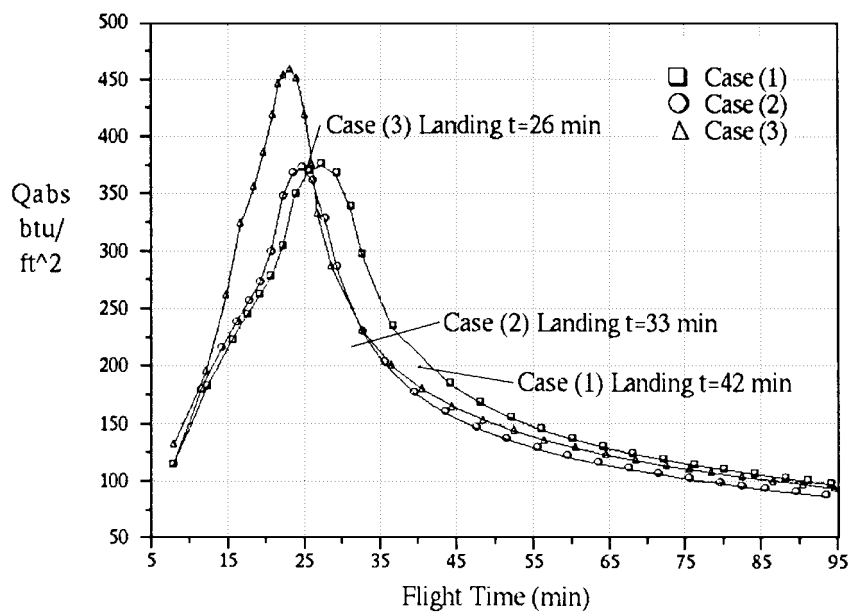

Fig. 8 Thermal energy absorbed at the vehicle surface vs flight time (tile TPS).

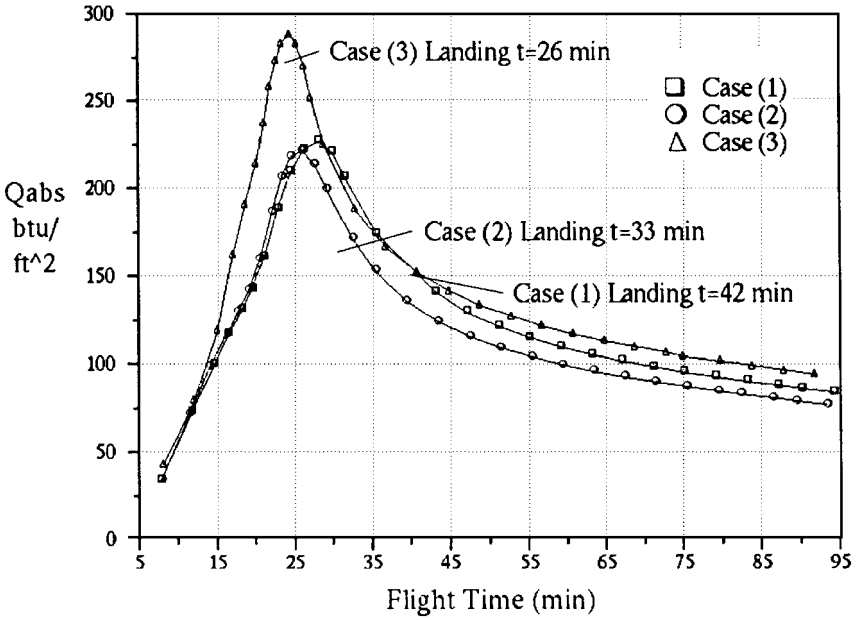

Fig. 9 Thermal energy absorbed at the vehicle surface vs flight time (blanket TPS).

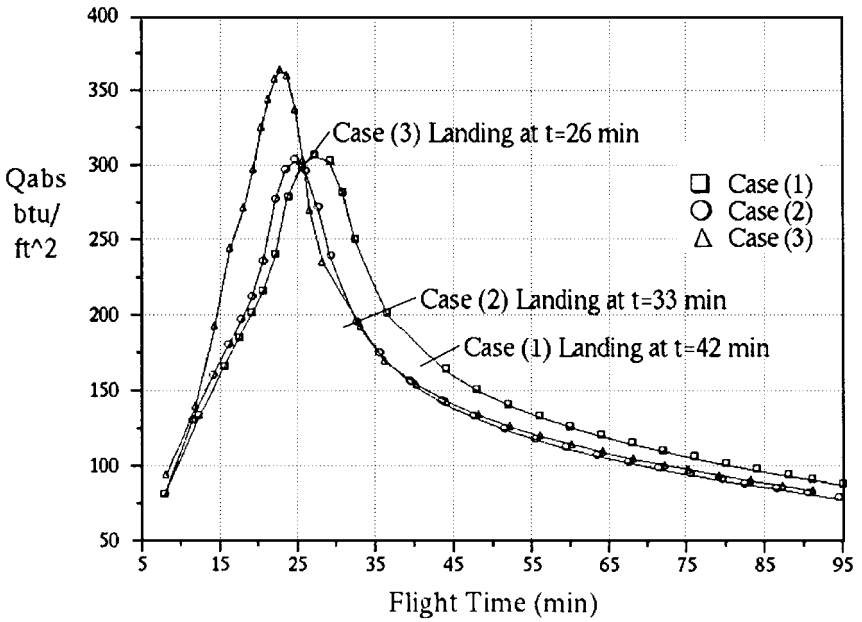

Fig. 10 Thermal energy absorbed at the vehicle surface vs flight time (metallic TPS).

Although the shapes of the curves are similar, the magnitude of the thermal energy absorbed at the vehicle surface differs depending on the TPS concept used. Also according to the figures, at a certain point in the trajectory Q_{abs} at the vehicle surface peaks. Past this point the vehicle surface temperature is so high that $\dot{Q}_{rad}$ has exceeded $\dot{Q}_{conv}$ [see Eq. (15)]. From then on the vehicle loses thermal energy and surface temperatures cool. This process continues well after the vehicle has landed.

Figures 11–13 show the time histories of internal structure temperatures. It is seen that case 2 gives the lowest maximum temperature. Also of interest is the fact that the internal structure temperature peaks well after landing in all cases. This directly contrasts with the surface temperature, which peaked with Q_{abs} earlier in the trajectory and is still cooling after landing. This transient heating effect is illustrated in Fig. 14. Notice that after the maximum surface temperature has been reached a heat pulse forms and begins traveling from the TPS surface to the vehicle structure. This heat pulse continues to increase the vehicle structure temperature even after the vehicle has landed.

Because it is desired to keep internal structure temperatures below 250°F, Table 3 shows that all of the TPS would have to be resized to meet this objective, particularly the metallic system. In general, the analysis developed in this paper will be an effective tool for sizing any TPS to any temperature requirement.

Other Options

The 3000°F stagnation temperature constraint is based on a carbon carbon nose cap material, which is currently used on the Space Shuttle. A new nose cap material made from zirconium diborites is under developement at NASA Ames Research Center. The new material can withstand temperatures in excess of 4000°F and motivates considering case 3*.

The case 3 trajectory lies on the maximum nose cap stagnation temperature boundary of the flight envelope for the first portion of the descent. If this condition is relaxed from 3000 to 4000°F, a significant improvement results. Case 3 and this case labeled 3* are compared in Fig. 15 for the tile TPS. Case 3* gives a trajectory that rapidly dives to the new nose cap stagnation temperature boundary

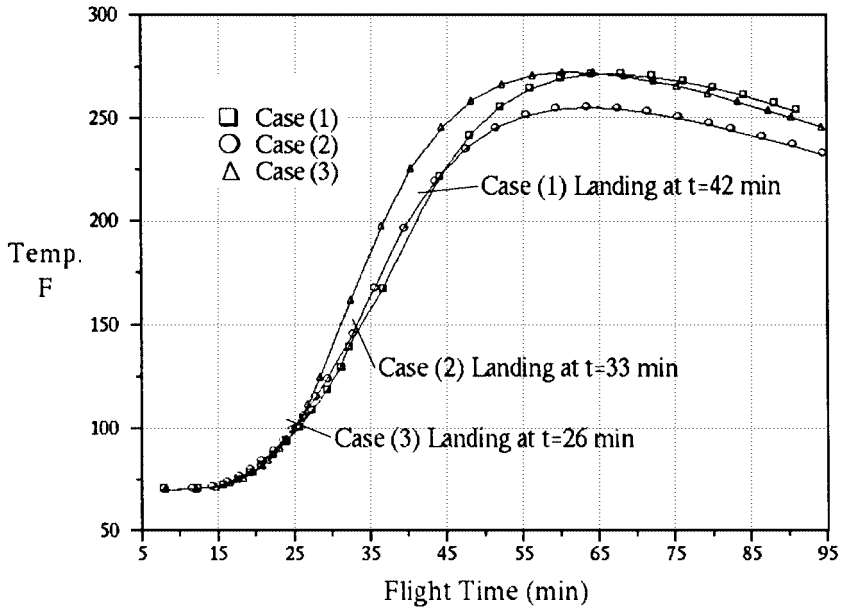

Fig. 11 Vehicle structure temperature vs flight time (tile TPS).

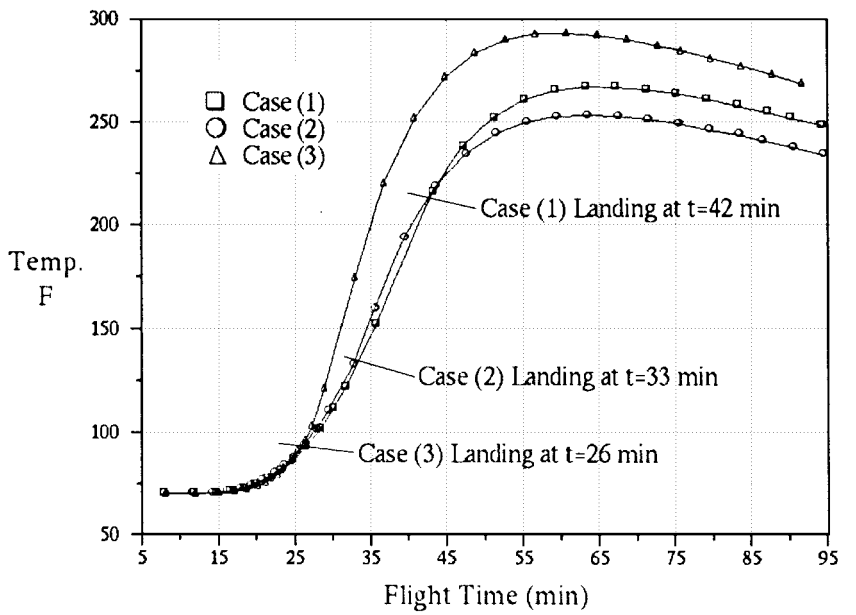

Fig. 12 Vehicle structure temperature vs flight time (blanket TPS).

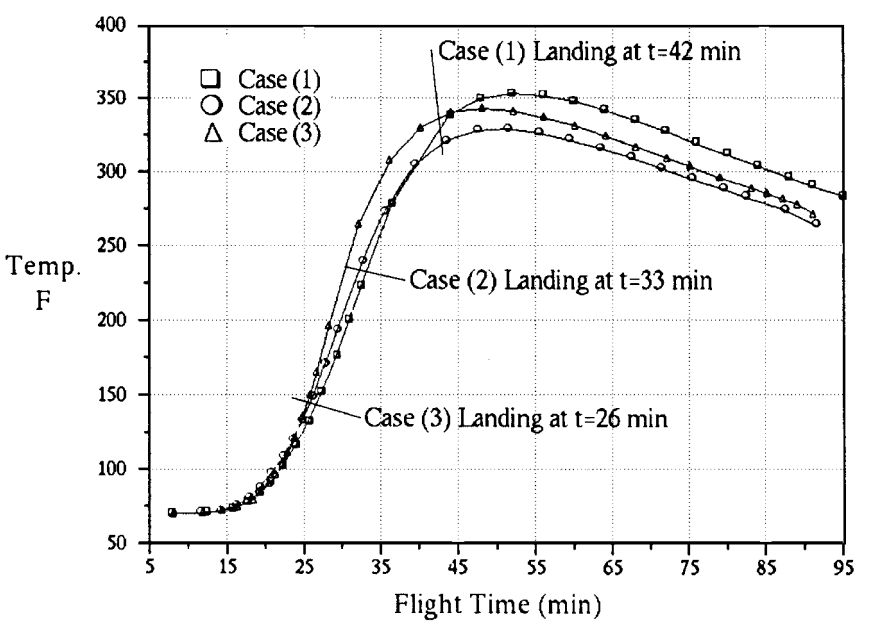

Fig. 13 Vehicle structure temperature vs flight time (metallic TPS).

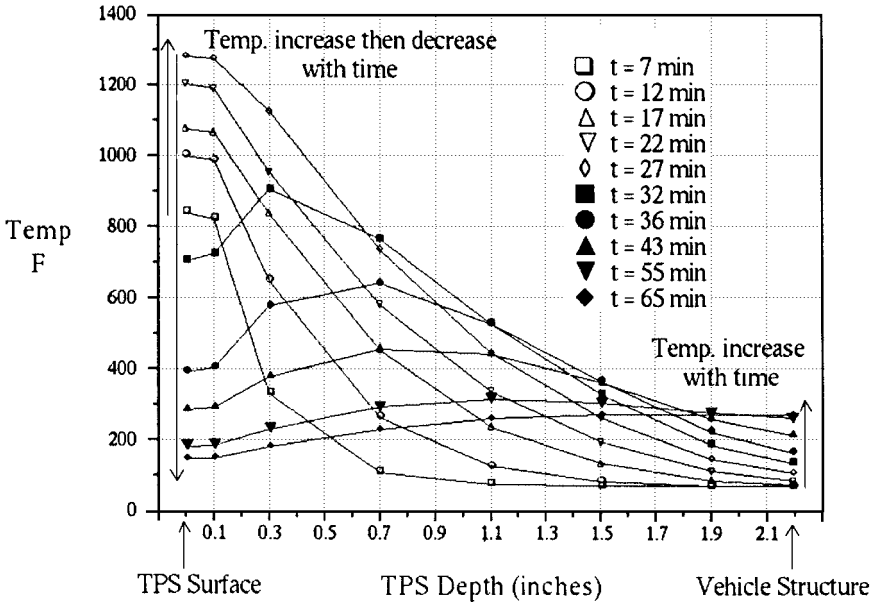

Fig. 14 TPS temperature profiles at different flight times (tile TPS, case 1).

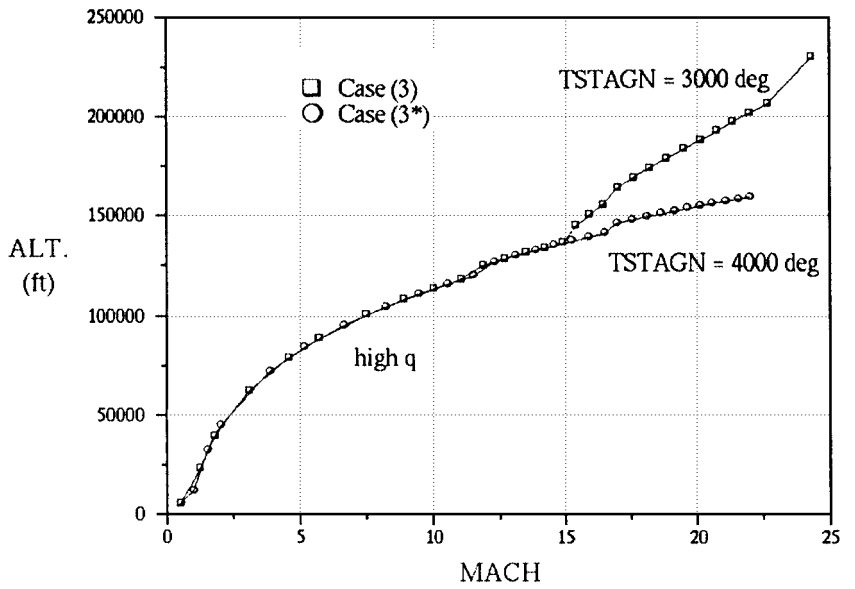

Fig. 15 Altitude vs Mach number (tile TPS).

(the load factor constraint was ignored for this dive) and remains in the high q region for the rest of the flight. Table 3 and Fig. 16 show that this trajectory not only has the minimum flight duration but also the lowest peak internal structure temperature as well, by a substantial 37°F relative to case 3 and by 25°F relative to case 2. Thus the use of this trajectory requires a smaller TPS thickness, giving a significant decrease in TPS weight. Surprisingly, even though case 3* produces the lowest peak internal structure temperature, it does not produce the lowest heat load. In fact, Table 3 shows that the case 3* heat load is high when compared with the heat loads produced by the low q trajectories. This relatively high heat load indicates that the benefits resulting from the case 3* trajectory are not predicted by minimizing heat loads.

The superiority of case 3* is due to two factors. First, the amount of time the vehicle undergoes convective heating determines how far the heat will diffuse into the TPS. A short descent time and a TPS with low thermal diffusivity does not allow the heat to diffuse into the TPS very far. Constraining the heat near the surface of the TPS makes a shorter path for the heat to radiate back out of the vehicle instead of continuing to conduct farther into the vehicle structure. Second, the high T_{surf} caused by a case 3* optimal trajectory increases the heat rejection rate $\dot{Q}_{rad}$ by T_{surf} to the fourth power; see Eq. (5). Thus, although the case 3* trajectory induces higher heat absorption rates on the vehicle, it allows even higher heat rejection rates. The combined effect of the short descent time and increased efficiency of heat rejection keeps the heat at the TPS surface, rejects the heat quickly, and reduces conduction into the vehicle structure, thereby minimizing the peak structure temperature of the vehicle. These combined effects are illustrated in Fig. 17, which shows TPS temperature profiles for each case at the time when peak surface temperatures occurred. Notice that the case 3* profile has the highest surface temperature and the smallest amount of heat diffusion.

Chattering trajectories were also considered. In these trajectories, the vehicle rapidly banks alternately left and right so that its flight path remains straight. This banking maneuver increases the vehicle lift and hence its drag. Although chattering drastically reduces descent time by increasing drag, it also increases $\dot{Q}_{conv}$, thereby increasing T_{surf}. Because the vehicle is constrained by TSTAGN already during the first half of its descent, chattering does not significantly change the case 3 optimal trajectory.

Trajectories were also generated minimizing the integral of T_{surf} with respect to time. This optimization integral is proportional to the integral of the steady-state conductive heat rate of the vehicle, assuming the vehicle tank wall temperature remains constant:

$$\dot{Q}_{steady} = (k/L)(T_{surf} - T_{tank,wall}) \tag{23}$$

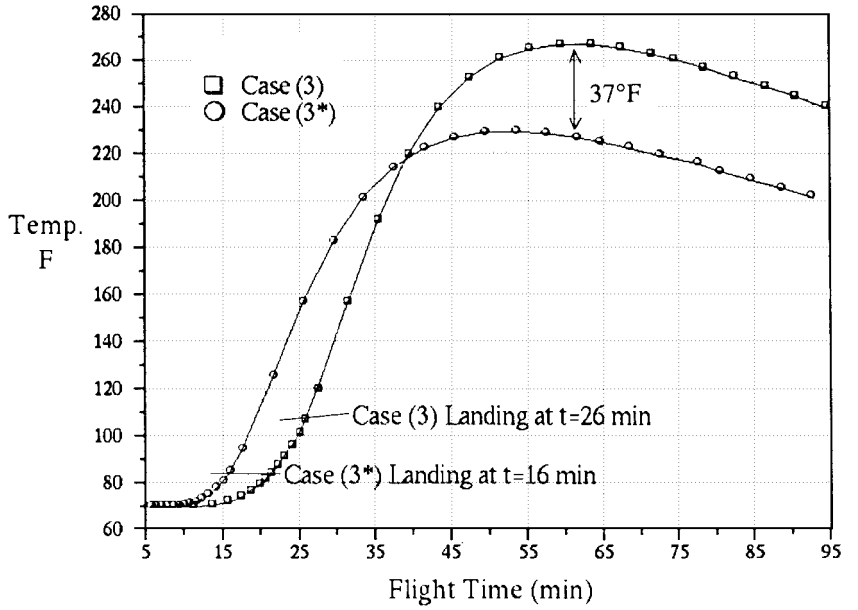

Fig. 16 Vehicle structure temperature vs flight time (tile TPS).

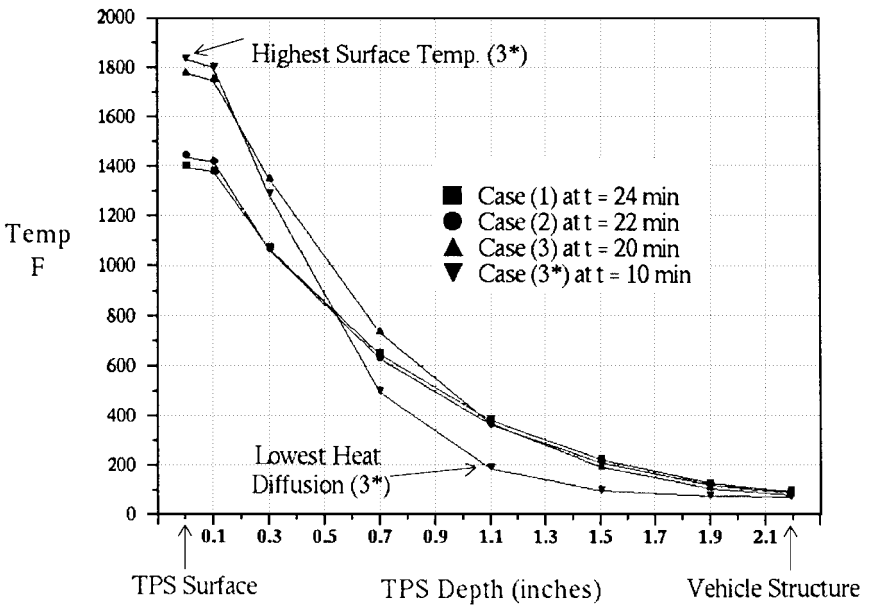

Fig. 17 TPS temperature profile at flight time of peak surface temperature (tile TPS).

The integral $T_{surf}\,dt$ optimal trajectory (not shown here) continually jumps between high q trajectories and low q trajectories. This is because T_{surf} and dt are now weighted equally, and low q trajectories minimize T_{surf} and high q trajectories minimize dt. Although jumping from one path to another is physically impossible, it is allowable by the ESA method. Constraining the trajectory with load factor limits eliminates the jumps but destroys the optimality of the trajectory. For example, a constrained integral $T_{surf}\,dt$ trajectory that starts out as a low q trajectory is forced to remain a low q trajectory because of the load factor constraint. On the other hand, the integral $T_{surf}\,dt$ trajectory could be forced to follow the high q trajectory at first, and it would remain on that trajectory due to the load factor constraint.

Concluding Remarks

Control volume heat transfer equations have been coupled to the entry flight dynamics equations for the purpose of determining trajectories that minimize thermal energy absorption and internal structure temperatures. The energy state approximation was used to obtain the near-optimal paths. The method may be used to size TPS and thereby provide estimates of the TPS weight.

It was found that the trajectories were of two types: very low dynamic pressure q and very high q. The low q trajectories have lower surface temperatures and higher descent times than do the high q ones. The low q trajectories gave lower peak internal structure temperatures, but the difference was very small. If TPS materials capable of withstanding higher surface temperatures are developed, then the high q trajectories become superior, giving substantially reduced internal structure temperatures for the same TPS. This reduction in peak internal structure temperature would allow a significant reduction in TPS weight for the same structure temperature constraint.

The peak internal structure temperatures for trajectories constrained by the 3000°F stagnation temperature limit were all very close together, with the trajectory minimizing heat load resulting in the minimum. Therefore minimizing the integral of T_{surf}^4 is a good approximation if the 3000°F limit cannot be violated. If stagnation temperatures beyond 3000°F are allowable, then transient temperature effects and heat conduction in the TPS play an important role in determining peak internal structure temperature, and trajectories minimizing heat load no longer result in the lowest peak internal

structure temperature. For this case the desired criterion is minimizing the thermal energy absorbed by the internal structure.

Finally, we note that the technique developed in this paper is noniterative and has modest computational requirements. Thus it could be used as an onboard guidance scheme to generate minimum heating trajectories in real time.

Acknowledgment

This research was supported by NASA Ames Research Center Grant NCC2-5165.

References

[1]Chow, H. C., Ardema, M. D., and Bowles, J. V., "Near Optimal Re-Entry Trajectories for Reusable Launch Vehicles," AIAA Paper 97-3582, Aug. 1997.

[2]Ardema, M. D., Bowles, J. V., and Whittaker, T., "Optimal Trajectories for Hypersonic Launch Vehicles," *Dynamics and Control*, Vol. 4, No. 4, 1994, pp. 337–347.

[3]Ardema, M. D., Bowles, J. V., Terjesen, E. J., and Whittaker, T., "Approximate Altitude Transitions for High-Speed Aircraft," *Journal of Guidance, Control, and Dynamics*, Vol. 18, No. 3, 1995, pp. 561–566.

[4]Ardema, M. D., Bowles, J. V., and Whittaker, T., "Near-Optimal Propulsion-System Operation for an Air-Breathing Launch Vehicle," *Journal of Spacecraft and Rockets*, Vol. 32, No. 6, 1995, pp. 951–956.

[5]Ardema, M. D., Chow, H.-C., and Bowles, J. V., "Near-Optimal Operation of Dual-Fuel Launch Vehicles," *Journal of Guidance, Control, and Dynamics*, Vol. 19, No. 5, 1996, pp. 1180–1182.

[6]Sachs, G., and Dinkelmann, M., "Heat Input Reduction in Hypersonic Flight by Optimal Trajectory Control," AIAA Paper 96-3905, July 1996.

[7]Patankar, S. V., *Numerical Heat Transfer and Fluid Flow*, 1st ed., Hemisphere, 1980, pp. 41–77.

[8]Olynick, D. R., and Tam, T., "Trajectory Based Validation of the Shuttle Heating Environment," AIAA Paper 96-1891, June 1996.

T. C. Lin
Associate Editor